REPORT DOCUMENTATION PAGE

Form Approved OMB NO. 0704-0188

1. REPORT DATE (DD-MM-YYYY)	2. REPORT TYPE	3. DATES COVERED (From - To)
04-11-2015	Final Report	1-Jan-2015 - 30-Sep-2015

4. TITLE AND SUBTITLE
Final Report: Novel Deployment of Mobile Eddy Covariance Tower Observations Across Variations in the Built Environment in a Desert Urban Area

5a. CONTRACT NUMBER
W911NF-14-1-0683

5b. GRANT NUMBER

5c. PROGRAM ELEMENT NUMBER
611102

6. AUTHORS
Enrique R. Vivoni, Nicole A. Pierini, Adam Schreiner-McGraw, Ivan Lopez-Castrillo

5d. PROJECT NUMBER

5e. TASK NUMBER

5f. WORK UNIT NUMBER

7. PERFORMING ORGANIZATION NAMES AND ADDRESSES
Arizona State University
ORSPA
AZ Board of Regents on behalf of Arizona State Unive
Tempe, AZ

8. PERFORMING ORGANIZATION REPORT NUMBER

9. SPONSORING/MONITORING AGENCY NAME(S) AND ADDRESS (ES)
U.S. Army Research Office
P.O. Box 12211
Research Triangle Park, NC 27709-2211

10. SPONSOR/MONITOR'S ACRONYM(S)
ARO

11. SPONSOR/MONITOR'S REPORT NUMBER(S)
65962-EV-II.1

12. DISTRIBUTION AVAILIBILITY STATEMENT
Approved for Public Release; Distribution Unlimited

13. SUPPLEMENTARY NOTES
The views, opinions and/or findings contained in this report are those of the author(s) and should not contrued as an official Department of the Army position, policy or decision, unless so designated by other documentation.

14. ABSTRACT
A mobile eddy covariance tower platform is used to analyze water and energy fluxes over three unique urban land cover representations on the Arizona State University campuses: (1) xeric landscape (gravel cover and palo verde trees with drip-irrigation systems near tall buildings); (2) high-density urban site (asphalt-paved parking lot near a high-traffic intersection); and 3) suburban mesic landscape (turf grass with sprinkler irrigation in a residential neighborhood). The footprints associated with the eddy covariance flux measurements are determined and image analysis allows for land cover classification of each source area. The xeric site and high-density urban site behave

15. SUBJECT TERMS
urban energy balance, mobile platform, irrigation, evapotranspiration, heat fluxes, urban materials

16. SECURITY CLASSIFICATION OF:			17. LIMITATION OF ABSTRACT	15. NUMBER OF PAGES	19a. NAME OF RESPONSIBLE PERSON
a. REPORT	b. ABSTRACT	c. THIS PAGE			Enrique Vivoni
UU	UU	UU	UU		19b. TELEPHONE NUMBER: 480-727-3575

Report Title

Final Report: Novel Deployment of Mobile Eddy Covariance Tower Observations Across Variations in the Built Environment in a Desert Urban Area

ABSTRACT

A mobile eddy covariance tower platform is used to analyze water and energy fluxes over three unique urban land cover representations on the Arizona State University campuses: (1) xeric landscape (gravel cover and palo verde trees with drip-irrigation systems near tall buildings); (2) high-density urban site (asphalt-paved parking lot near a high-traffic intersection); and 3) suburban mesic landscape (turf grass with sprinkler irrigation in a residential neighborhood). The footprints associated with the eddy covariance flux measurements are determined and image analysis allows for land cover classification of each source area. The xeric site and high-density urban site behave like a semiarid landscape, with high Bowen ratios (~3 and ~8 respectively) and higher sensible heat fluxes. The mesic site behaves more similarly to a grassland, with a Bowen ratio of ~0.5 and latent heat flux greater than sensible heat flux. Precipitation events affects latent heat flux at the xeric site, while the high-density urban site appears to be relatively insensitive to precipitation input. Differences are observed in evaporative fraction, Bowen ratio, and the ratios of sensible heat and latent heat to the available energy when comparing wet days to dry days. There is also a difference observed when only rainfall events occurring during the day-time are considered, suggesting the timing of precipitation influences the urban surface energy and water balances. This analysis improves our understanding of energy and water fluxes over desert urban land covers and provides a framework for future assessments.

Enter List of papers submitted or published that acknowledge ARO support from the start of the project to the date of this printing. List the papers, including journal references, in the following categories:

(a) Papers published in peer-reviewed journals (N/A for none)

Received Paper

TOTAL:

Number of Papers published in peer-reviewed journals:

(b) Papers published in non-peer-reviewed journals (N/A for none)

Received Paper

TOTAL:

Number of Papers published in non peer-reviewed journals:

(c) Presentations

Lopez-Castrillo, I. and Vivoni, E.R. 2015. Urban Meteorological Flux Measurements using a New Mobile Platform. ASU FURI Symposium, Tempe, AZ.

Pierini, N.A., Vivoni, E.R., Lopez-Castrillo, I., and Schreiner-McGraw, A.P. 2015. Evaluating Water and Energy Fluxes across Three Land Cover Types in a Desert Urban Environment Through a Mobile Eddy Covariance Platform. American Geophysical Union Fall Meeting, San Francisco, CA.

Number of Presentations: 2.00

Non Peer-Reviewed Conference Proceeding publications (other than abstracts):

Received	Paper

TOTAL:

Number of Non Peer-Reviewed Conference Proceeding publications (other than abstracts):

Peer-Reviewed Conference Proceeding publications (other than abstracts):

Received	Paper

TOTAL:

Number of Peer-Reviewed Conference Proceeding publications (other than abstracts):

(d) Manuscripts

Received	Paper

TOTAL:

Number of Manuscripts:

Books

Received Book

TOTAL:

Received Book Chapter

TOTAL:

Patents Submitted

Patents Awarded

Awards

US Frontiers of Engineering Participant, National Academy of Engineering, 2015.
Visiting Sabbatical Researcher, Mexican Council of Science and Technology, 2015-2016.
Distinguished Visiting Professor, Mexican Academy of Sciences, 2015.
Leopold Leadership Fellow, Woods Institute for the Environment, Stanford University, 2015-2016.

Graduate Students

NAME	PERCENT_SUPPORTED	Discipline
Nicole Pierini	0.50	
Adam Schreiner-McGraw	0.50	
FTE Equivalent:	**1.00**	
Total Number:	**2**	

Names of Post Doctorates

NAME	PERCENT_SUPPORTED
FTE Equivalent:	
Total Number:	

Names of Faculty Supported

NAME	PERCENT_SUPPORTED	National Academy Member
Enrique Vivoni	0.00	
FTE Equivalent:	**0.00**	
Total Number:	**1**	

Names of Under Graduate students supported

NAME	PERCENT_SUPPORTED	Discipline
Ivan Lopez-Catrillo	0.25	Civil and Environmental Engineering
FTE Equivalent:	**0.25**	
Total Number:	**1**	

Student Metrics

This section only applies to graduating undergraduates supported by this agreement in this reporting period

The number of undergraduates funded by this agreement who graduated during this period: 1.00

The number of undergraduates funded by this agreement who graduated during this period with a degree in science, mathematics, engineering, or technology fields:..... 1.00

The number of undergraduates funded by your agreement who graduated during this period and will continue to pursue a graduate or Ph.D. degree in science, mathematics, engineering, or technology fields:..... 1.00

Number of graduating undergraduates who achieved a 3.5 GPA to 4.0 (4.0 max scale):..... 1.00

Number of graduating undergraduates funded by a DoD funded Center of Excellence grant for Education, Research and Engineering:..... 0.00

The number of undergraduates funded by your agreement who graduated during this period and intend to work for the Department of Defense 0.00

The number of undergraduates funded by your agreement who graduated during this period and will receive scholarships or fellowships for further studies in science, mathematics, engineering or technology fields: 0.00

Names of Personnel receiving masters degrees

NAME
Total Number:

Names of personnel receiving PHDs

NAME
Total Number:

Names of other research staff

NAME	PERCENT_SUPPORTED

FTE Equivalent:
Total Number:

Sub Contractors (DD882)

Inventions (DD882)

Scientific Progress

See attachment

Technology Transfer

Novel Deployment of Mobile Eddy Covariance Tower Observations Across Variations in the Built Environment in a Desert Urban Area

Enrique R. Vivoni, Nicole A. Pierini, Adam P. Schreiner-McGraw and Ivan Lopez-Castrillo

School of Sustainable Engineering and the Built Environment
School of Earth and Space Exploration
Arizona State University
Tempe, AZ

Final Report to Army Research Office
Project 65962EVII

November 3, 2015

Table of Contents

1. Introduction 3

2. Methods 4
    2.1. Study Sites and Characteristics 4
    2.2. Land Cover Classifications 5
    2.3. Mobile Eddy Covariance Tower Platform and Flux Processing 6
    2.4. Footprint Analysis 7

3. Results and Discussion 8
    3.1. Footprint Representation of Land Cover 8
    3.2. Hydrologic Dynamics Across Variable Seasons 9
    3.3. Comparison of Urban Surface Fluxes 12

4. Summary and Conclusions 15

References 16

Figure Captions 18

Table Captions 30

1. Introduction

Urbanization transforms a natural landscape into a built environment, thus affecting the energy and water balances across multiple spatial and temporal scales [e.g., *Georgescu et al*., 2009; *Lee et al*., 2012; *Chow et al.*, 2014]. Urban areas are comprised of construction materials (concrete, asphalt, gravel cover, etc.), vegetation of different types (native and non-native, with or without irrigation), and transportation and industrial activities. Each uniquely impacts the water and energy exchanges between the urban surface and the overlying atmosphere.

Urban water and energy exchanges can be particularly important in desert cities, such as Phoenix, Arizona, which naturally would be a water-limited ecosystem of the Sonoran Desert. However, urban development leads to the introduction of outdoor water use [*Gober et al.*, 2010; *Volo et al.*, 2014], which alters the water balance. Similarly, the urban heat island (UHI) effect alters the energy balance. Urban water and energy fluxes between the surface and atmosphere are controlled by land surface characteristics [*Oke et al.*, 2006].

The eddy covariance method is a popular technique to measure water, energy, and carbon fluxes over a local scale. Recent studies have used the eddy covariance method to measure urban surface energy balance [e.g. *Grimmond and Christen*, 2012; *Chow et al.*, 2014; *Crawford and Christen*, 2015]. The eddy covariance footprint is the surface area influencing the flux measurements, and constantly changes as a function of wind direction, atmospheric stability, and lateral dispersion qualities of the flow [*Schmid*, 1994]. A major challenge remains in quantifying how land surface characteristics within the eddy covariance footprint impact the flux measurements [*Loridan and Grimmond*, 2012]

In this study, a mobile eddy covariance platform is deployed at three urban settings located on Arizona State University (ASU) campuses representing three urban land cover types:

(1) xeric landscape (gravel cover and palo verde trees with drip-irrigation systems near tall buildings); (2) high-density urban site (asphalt-paved parking lot near a high-traffic intersection); and 3) suburban mesic landscape (turf grass with sprinkler irrigation in a residential neighborhood). The objectives are to: (a) measure energy, water and carbon fluxes across different land surface types; (b) quantify the tower footprint extent to identify contributing source areas to the flux measurements; and (c) analyze the differential response to precipitation and irrigation input at the various land cover sites. This analysis will improve our understanding of how energy and water fluxes vary across desert urban areas.

2. Methods

2.1. Study Sites and Characteristics

The three sites in this study are located on ASU property (Table 1), representing common urban landscapes observed in the Phoenix metropolitan area. The first site was established in a xeric landscape on the ASU Tempe campus (Fig. 1a,b). The xeric landscape is composed of palo verde trees with gravel and bare soil. The palo verde trees are regularly irrigated using a drip irrigation system and are approximately 3 to 5 meters tall. The duration of the mobile eddy covariance tower (ECT) deployment at the palo verde site (PV-ECT) was 53 days from January 20, 2015 to March 13, 2015. The second site was established on the ASU Tempe campus in a parking lot, with a large extent of paved surfaces (Fig. 1c,d). The duration of the parking lot mobile eddy covariance tower (PL-ECT) deployment was 43 days from May 19, 2015 to June 30, 2015. The third site was established near residences on the ASU Polytechnic campus in Mesa, Arizona, to represent a mesic landscape (Fig. 1e,f). The landscape consists of turf grass, which is regularly irrigated using overhead sprinklers three times per week and mowed two times

per week. The duration of the turf grass mobile eddy covariance tower deployment (TG-ECT) was 74 days from July 9, 2015 to September 18, 2015.

Following *Stewart and Oke* [2012], each site is classified to a Local Climate Zone (LCZ) to qualitatively describe its characteristics. PV-ECT associates with LCZ C, which has a zone function of natural scrubland and is defined as an open arrangement of bushes, shrubs, and short, woody trees. PL-ECT is described with LCZ E, which is defined as a featureless landscape of rock or paved cover, few or no trees or plants. Its zone function is a natural desert or urban transportation. TG-ECT is described with LCZ 6, defined as an open arrangement of low-rise buildings and an abundance of pervious land cover (low plants and scattered trees).

The climate of Phoenix, AZ and Mesa, AZ is classified as a hot arid subtropical desert (Köppen climate classification *BWh*). Average annual temperature is 75°F and 71°F in Phoenix and Mesa, respectively. Precipitation is bimodal, occurring predominantly during the winter (December to February) with low intensity and longer duration storms, and the summer (July to September) with short, high intensity storms, which are representative of the North American monsoon (NAM) [*Adams and Comrie*, 1997]. Average annual precipitation is approximately 210 mm/yr in Phoenix and approximately 235 mm/yr in Mesa.

2.2. Land Cover Classifications

Each site represents a different pattern of distinct urban land cover features. A land cover classification was performed on high-resolution (1 foot) orthoimagery obtained from the U.S. Geological Survey. Classifications were based on the Red, Green, and Blue (RGB) bands of the orthoimagery using a maximum likelihood classification that utilized training samples that were verified with ground observations. Land cover was classified into five types for the PV-ECT (Fig. 2c) and PL-ECT (Fig. 3c) sites, and six types for the TG-ECT site (Fig. 4c): Trees; Grass;

Undeveloped-Open Land (generally gravel or bare soil); Pavement; Buildings and Concrete; and Residential Buildings (TG-ECT site only). Buildings and concrete were classified together since both appear gray-white in the imagery. Trees, grass, and undeveloped-open land represent pervious surfaces, while pavement, buildings and concrete, and residential buildings represent impervious surfaces.

2.3. Mobile Eddy Covariance Tower Platform and Flux Processing

The mobile eddy covariance (EC) tower platform consists of a telescoping tower mounted on a trailer that can extend to a height of 15 meters. The tower was set at different heights among the three different land surfaces to attempt to measure fluxes above the canopy or building heights in its fetch, yet maintain a relatively small footprint so that the land cover of interest comprised the majority of the tower fetch (Table 2). Instruments are mounted to measure meteorological fluxes between the urban surface and atmosphere, including: barometric pressure (CS100, Setra); air temperature and humidity at three different heights (near ground surface ~0.3 m, ~0.5*height of EC instruments, and ~height of EC instruments), (HMP155A, Vaisala); incoming solar radiation at 5 m height (CMP3, Kipp & Zonen); net incoming and outgoing longwave and shortwave radiation at 5 m height (CNR4, Kipp & Zonen); incoming and outgoing photosynthetic active radiation (PAR) (SQ-110, Apogee Instruments Inc.); incoming and outgoing shortwave radiation (SP-110, Apogee Instruments Inc.); CO_2 and H_2O concentrations using an open-path Infrared Gas Analyzer (LI7500A, LI-COR); and three-dimensional wind velocity (CSAT3, Campbell Sci.) at 7, 8 or 9 m height aligned to the dominant wind direction of the season as determined by wind rose diagrams from nearby meteorological stations (Table 2). Soil conditions are evaluated with measurements of: surface temperature (SI-111, Apogee Instruments Inc.); soil moisture at 5, 15, and 50 cm depths (CS616, Campbell Sci.); soil

temperature at 2 and 4 cm depths (TCAV, Campbell Sci.); and soil heat flux at 5 cm depth (HFP01-SC, Hukseflux). Soil moisture, soil temperature and soil heat flux were not measured at the PL-ECT site as the tower was measuring a paved surface. EC data were sampled at a 20 Hz frequency for the PV-ECT site and at 10 Hz frequency for the PL-ECT and TG-ECT sites and recorded by a datalogger (CR5000, Campbell Sci. or CR3000, Campbell Sci.).

Fluxes were processed using EdiRE (University of Edinburgh), which includes correction for fluctuations in stability [*Foken et* al., 2006] and density [*Webb et al.*, 1980], sonic temperature use to calculate sensible heat flux, rotating the coordinate frame to set the mean vertical wind speed to zero [*Wilczak et al.*, 2001], and removing signal lag in gas concentrations [*Massman*, 2001]. Flux data was filtered to exclude time periods when there was precipitation, the wind direction was 180˚ ± 10˚ from the direction at which the EC instruments were mounted due to possible interference from the tower setup, and for outliers greater than 3 standard deviations. Other measurements were recorded by a datalogger (CR5000, Campbell Sci. or CR3000, Campbell Sci.) as averages every 30 minutes.

2.4. Footprint Analysis

Eddy covariance measurements were used to estimate the footprint, or source area, of the measured turbulent fluxes [*Gash*, 1985; *Schmid*, 1997]. The analytical model from *Kormann and Meixner* [2001] was used to calculate the footprint for an area of 600 meters by 600 meters, centered at each ECT. The horizontal resolution of the footprint contributions was set to 3 meters, which is less than the measurement heights [*Van de Boer et al.*, 2013; *Anderson and Vivoni*, 2015]. The footprint calculations were processed using EDiRE, and depend on measurement height, mean horizontal wind velocity, wind direction, friction velocity, Monin-Ohbukov stability, and the standard deviation of the lateral wind velocity. Lower limits of wind

velocity, friction velocity, stability and sensible heat flux were set to ensure footprints were calculated during turbulent daytime conditions. Footprints were estimated at 30 minute time intervals and then averaged at a daily scale. The daily averaged footprints were then used to derive a unique deployment period averaged footprint for each ECT.

Source area represents the area around each ECT that contributes to the flux measurements. In this study, the 50% source area and the 80% source area are evaluated. The 50% source area is defined as the area that is responsible for 50% of the surface influence, with regards to the flux measurements [*Schmid*, 1994]. The area that accounts for 80% of the surface influence is referred to as the 80% source area.

3. Results and Discussion

3.1. Footprint Representation of Land Cover

Land cover classification was performed using 1 foot resolution orthoimagery centered at each ECT. To quantify the land cover types that were contributing to the flux measurements, the 50% source areas were calculated for each ECT. The 80% source areas were calculated for PV-ECT and PL-ECT, however the 600 meter by 600 meter box centered at the TG-ECT did not account for at least 80% of the flux measurements at the site. This could be improved in a future effort by defining a larger fetch. The percent of area that was accounted for in the 300 meter fetch (or 600 meter by 600 meter box) is 96.2%, 90.1% and 61.1% for the PV-ECT, PL-ECT, and TG-ECT, respectively. As a result, the 50% source areas are used to quantitatively compare land class distribution among the three sites in this study (Table 3).

The PV-ECT site (Fig. 2b,c) has a relatively small 50% source area (1,917 m^2). Trees, specifically palo verde trees, dominate the land cover at 56%. The next dominant land cover is undeveloped (bare soil or gravel) at 37%. Pavement, buildings and concrete, the impervious

materials, account for 7.8% together. When a larger source area is considered (80% source area), the land cover classes are more evenly distributed, with the footprint extending beyond the palo verde patch to surrounding buildings, concrete, and pavement. The PL-ECT site (Fig. 3b,c) has a larger 50% source area (9,243 m^2). The most dominant land class is pavement, as expected, at 83%. Undeveloped regions account for 10%. Trees and grass make up 4.5% with buildings and concrete at 2.5%. Again, the land cover classes are more evenly distributed when a larger source area is considered, however pavement still dominates at 56% in the 80% source area. The TG-ECT site (Fig. 4b,c) is the most evenly distributed. It has the largest 50% source area of the three sites at 14,346 m^2. The land cover classifications are much more evenly distributed. The dominant land class is undeveloped (bare or gravel) land at 36.5% followed by grass cover at 23.6%. Trees account for 18%, pavement is 11.5% and then residential buildings comprise 8%. Building and concrete have the smallest areal percentage at 2.6%. Pervious land cover types comprise approximately 78% of the 50% source area.

3.2. Hydrologic Dynamics Across Variable Seasons

The PV-ECT deployment period was in the winter time, however it had the greatest amount of total rainfall (Table 4). The largest storm also had the longest duration (~1 day) and accumulated 23.8 mm between 18:00 on 1/29/2015 to 20:00 on 1/30/2015. In general the PV-ECT measured lower temperatures (surface and air) due to the season (Fig. 5a). Surface temperature had the highest variation and had much higher maximum daily temperature values. The surface temperature was measuring the temperature of the inter-canopy spaces which consists of gravel and bare soil. Incoming solar and net radiation were also the lowest of the three deployments because of the season (Fig. 5b). During rainfall events, incoming solar and net radiation decreased due to cloud cover. The PV-ECT generally also had high sensible heat fluxes

(Fig. 5c). There was one large increase in latent heat flux after the day long storm event at the end of January. This is expected as the moisture input was large and palo verde trees represent a large areal fraction of the footprint. A slight increase in latent heat flux was also observed after an early March rainfall event. Soil moisture was measured at two depths, 5 cm and 50 cm (Fig. 5d). The shallow depth has a slight response every day, which is assumed to be related to the drip irrigation, and a large response to precipitation input. The 50 cm depth remained relatively constant during the deployment period. This is expected because during the installation of the sensor, a black mesh isolating the lower soil was discovered at ~20 cm. The mesh will limit the amount of water that can infiltrate. This may also explain the increased latent heat flux after the long storm even in January. A large precipitation input coupled with the limited ability to infiltrate water could result in high surface evaporation rates.

The PL-ECT deployment period occurred from late May through June, which is typically the driest and hottest time of the year. Surface temperature was very high (Fig. 6a). The sensor was measuring the gravel that mobile ECT platform sat on, however temperatures measured were still very high, with peaks up to 68°C. Air temperature was relatively high, due to the time of year. The air temperature measurement at the 'high' height, approximately 9 m, had the lowest readings, with the air temperature measurement closest to the surface giving the highest readings. Incoming solar radiation and net radiation were relatively high (Fig. 6b). During the precipitation event in early June, temperatures, incoming solar and net radiation all decreased. Latent heat flux also increased slightly following the early June rainfall event (Fig. 6c). However, sensible heat flux was dominant for the entire deployment period, largely due to concrete representing a large majority of the ECT footprint. Ground heat flux could not be measured at the site. Interestingly, there is not a large change in any of the measured variables to the precipitation events that

occurred on June 27 and June 29. This may be because both events occurred at night, and both were short with high intensity. It is possible that summer-type storms have a small temporal impact on pavement land cover with regards to flux measurements.

The TG-ECT deployment occurred during the NAM season, from mid-July to mid-September. Surprisingly however, there was relatively little rainfall recorded during the period (Table 4). In contrast to the other two sites, surface temperature was lower than air temperature, corresponding to the irrigated turf grass (Fig. 7a). As the air temperature was taken at increasing heights, the air temperature measurements also increased. Incoming solar and net radiation were relatively high, as expected for the season (Fig. 7b). Also in contrast to the other two sites, latent heat flux was dominant (Fig. 7c). This is expected as the grass is regularly irrigated (three times per week). Latent heat flux appears to slightly increase after rainfall events. Soil moisture was measured at 5 cm, 15 cm, and 50 cm depths (Fig. 7d). All of the soil moisture values were high. The 5 cm and 15 cm soil moisture appears to vary ~3 times per week, mimicking the irrigation schedule. A deeper moisture pulse was observed with the rainfall event on 8/11/2015, which had 1.7 mm of measured precipitation. Otherwise, soil moisture at 50 cm was fairly constant.

The diurnal cycle for energy flux components was averaged at 30 minute time intervals for each site over each site's deployment time period (Fig. 9). PL-ECT has the highest net radiation, which is expected given the time of year for the deployment. At nighttime, PL-ECT also has the most negative net radiation. This is likely due to the outgoing longwave radiation correlated with the high surface temperature of the pavement. Sensible heat flux is fairly similar between the PV-ECT and the PL-ECT. There is a slight lag of peak sensible heat flux at PL-ECT, which occurs around 14:00. Sensible heat flux is lowest at TG-ECT. TG-ECT has the highest latent heat flux, which peaks around 12:00. PL-ECT has the lowest latent heat flux,

which peaks slightly around 13:00. Ground heat flux patterns are similar between PV-ECT and TG-ECT. Average rainfall is computed as the average amount of rainfall that fell during that 30 minute time period over the duration of the deployment. The one day long precipitation event during the PV-ECT deployment is evident in this calculation (Fig. 9a) because there is a contribution for almost every 30 minute period.

To evaluate the energy balance, the 30 minute averaged flux data was plotted with net radiation minus ground heat flux on the *x*-axis, and sensible heat flux plus latent heat flux on the *y*-axis. A linear regression was fit to each plot and the y-intercept and slope were calculated, following this equation: $LE+H=m(Rn-G)+b$. For PV-ECT, $y = 0.53x + 27$ with $R^2 = 0.90$. The result of the linear regression to evaluate the energy balance fit for TG-ECT is: $y = 0.72x + 33$ with $R^2 = 0.89$. This indicates that TG-ECT site has a better energy balance closure.

3.3. Comparison of Urban Surface Fluxes

To better compare the sites to one another, different energy flux ratios were evaluated. Evaporative fraction (*EF*) is computed at noon time of each day as $EF = LE/(LE+H)$, where *LE* is latent heat flux and *H* is sensible heat flux. Bowen ratio (*B*) is computed at noon time of each day as $B = H/LE$. An average was taken of the computed *EF* and *B* over each site's deployment period and they are summarized in Table 5. Ratios of sensible heat to net radiation minus ground heat flux and latent heat to net radiation minus ground heat flux were also computed at a daily average time step (Fig. 10), and will be referred to as the sensible heat ratio and latent heat ratio, respectively. The average over all of the days in each site's deployment period was calculated (Table 5). On average, evaporative fraction was highest at TG-ECT, followed by PV-ECT and then PL-ECT. This is expected due to the high measured latent heat fluxes at the turf grass site, and the very low latent heat fluxes at the parking lot site. Bowen ratio is ~3 at PV-ECT and ~8 at

PL-ECT, which are representative of a semi-arid to desert environment because sensible heat fluxes are high. Average *B* is 0.53 at TG-ECT, which means that latent heat flux is dominant. When evaluating the time series of the flux ratios, the rainfall events that occurred at PV-ECT are apparent. Sensible heat ratio is generally higher except for the few days around each rainfall event. At PL-ECT, both ratios are likely underestimated due to no ground heat flux measurement, therefore *G* was assumed to equal zero for the ratio calculation. The sensible heat ratio is always higher than the latent heat ratio. The difference between the two is fairly constant, but decreases during the rainfall event in early June. TG-ECT observes an opposite trend, as latent heat ratio is generally always higher than sensible heat ratio. However, the difference between the two is much more variable.

To further evaluate how the surfaces responded to precipitation input, *EF*, *B*, sensible heat and latent heat ratios were calculated for 'Wet', 'Dry', 'Wet Daytime' (abbreviated as 'Wet-Day'), and 'Dry Daytime' (abbreviated as 'Dry-Day') at averaged day periods (Table 6). 'Wet' days are defined as any day where precipitation occurred or a day where precipitation occurred within the last 3 days. Essentially averages were computed for the day of rainfall plus the three subsequent days after rainfall. 'Dry' days are defined as all other days during the deployment period that did not meet that criteria. 'Wet-Day' time steps are defined as days where precipitation occurs during day-time hours and three days after such a precipitation event. 'Dry-Day' is defined as all other days during the deployment period that do not meet the 'Wet-Day' criteria. In summary, PV-ECT has 18 and 33 wet and dry days, with 13 and 38 wet-day and dry-day time periods. PL-ECT has 9 and 32 wet and dry days, with 6 and 35 wet-day and dry-day time periods, and TG-ECT has 17 and 53 wet and dry days, with 7 and 63 wet-day and dry-day time periods. By differentiating wet and dry days, the patterns observed are strengthened. All

sites have an increased *EF* on wet days as compared to dry days, with the difference increasing the most at PL-ECT. The difference between *EF* is larger at all 3 sites when evaluating only day-time rainfall events. There is not a significant difference in computed *B* at PV-ECT when evaluating all rainfall events, however there is when evaluating day-time rainfall events, with a lower *B* for wet-day day periods. TG-ECT actually averages a higher *B* for wet periods when all rainfall events are considered, but only day-time rainfall events lead to a lower *B* for wet-days. Sensible heat ratios are lower for wet days and higher for dry days at PV-ECT and TG-ECT. Latent heat ratios are higher or wet days and lower for dry days at PV-ECT. The ratios appear to be largely dependent on moisture availability at PV-ECT. Interestingly, the sensible heat and latent heat ratios are both higher for wet days and wet-day daily periods compared to the dry values at PL-ECT. It is important to note that *G* is not measured at the PL-ECT, so the calculation is a fraction of sensible heat and latent heat to net radiation. TG-ECT is insensitive to latent heat flux, regardless of the days considered, which is likely due to the constant irrigation input. In general, wet time periods result in higher evaporative fractions, lower Bowen ratios, lower sensible heat ratios, and higher latent heat ratios. These trends are more pronounced when only day-time precipitation events are considered, suggesting that the timing of precipitation has an influence on how the surfaces respond to water and energy fluxes.

Carbon dioxide fluxes were calculated at 30 minute averages, and then averaged over a daily time step for each ECT site to observe general magnitudes (Fig. 11). Both PV-ECT and PL-ECT have positive CO_2 fluxes, indicating that CO_2 is being released into the atmosphere. This is likely a result of urban CO_2 sources. The TG-ECT site measures CO_2 fluxes that are generally negative, indicating the land surface may sequester carbon.

4. Summary and Conclusions

Urban water and energy exchanges between the surface and atmosphere are controlled by land surface characteristics. In this study, water and energy fluxes were evaluated at three different urban land cover representations. Comparisons between the three sites reveal:

(1) Surface temperature is higher than air temperature for PV-ECT and PL-ECT, whereas surface temperature is less than air temperature at TG-ECT.

(2) Sensible heat flux dominates at PV-ECT and PL-ECT, while latent heat flux dominates at TG-ECT. This is likely due to above ground sprinkler irrigated grass comprising a sizeable fraction of the TG-ECT footprint.

(3) PV-ECT site responds to long precipitation events with a spike in latent heat flux. The PL-ECT site appears to be relatively insensitive to rainfall events, however the sample size of precipitation events is small.

(4) Precipitation influences *B*, *EF*, sensible and latent heat ratios over all three land surfaces. Changes are more noticeable during day-time precipitation events, which may suggest that precipitation timing influence the surface response to energy and water fluxes.

The three different site deployments occurred during different times of the year, which limits the ability to compare fluxes from one site to another. Further data analysis can be useful to better understand difference between the three sites, including a direct comparison of the three sites with continuous data from an urban tower in Phoenix, as described by *Chow et al.* [2014], and a natural landscape tower in the Sonoran Desert, as described by *Pierini et al.* [2014]. As desert urban areas continue to grow, it is important to improve our understanding of how the energy and water balances vary across urban land cover.

References

Adams, D. K., and A. C. Comrie (1997), The North American Monsoon, *Bull. Amer. Meteorol. Soc.*, *78*(10), 2197 – 2213, doi:10.1175/1520-0477(1997)078<2197:TNAM>2.0.CO;2.

Anderson, C. A. (2013), *Assessing Land-Atmosphere Interactions through Distributed Footprint Sampling at Two Eddy Covariance Towers in Semiarid Ecosystems of the Southwestern U.S.* Masters of Science in Civil, Environmental and Sustainable Engineering, Arizona State University, 243 pp.

Anderson, C. A. and E. R. Vivoni (2015), Land surface states within the flux footprint impace land-atmosphere coupling in two semiarid ecosystems of the southwestern U.S., *Water Resour. Res.*, Submitted.

Chow, W. T. L., T. J. Volo, E. R. Vivoni, G. D. Jenerette and B. L. Ruddell (2014), Seasonal dynamics of a suburban energy balance in Phoenix, Arizona, *Int. J. Climatol.,* 34, 3863-3880, doi: 10.1002/joc.3947

Crawford, B. and A. Christen (2015), Spatial source attribution of measured urban eddy covariance CO_2 fluxes, *Theor. Appl. Climatol.*, 119, 733-755, doi:10.1007/s00704-014-1124-0.

Foken, T. (2006), 50 Years of the Monin-Obukhov similarity theory, *Boundary Layer Meteorology*, 119, 431 – 447.

Gash, J. H. C. (1986), A note on estimating the effect of limited fetch on micrometeorological evaporation measurements, *Bound. Layer Meteorol.*, 35, 409 – 413.

Georgescu, M. and G. Miguez-Macho (2009), Climatic effects of 30 years of landscape change over the Greater Phoenix, Arizona, region: 1. Surface energy budget changes, *J. Geophys. Res.*, 114, D05110.

Grimmond, C. S. B and A. Christen (2012), Flux measurements in urban ecosystems, *Fluxl. Newsl. Fluxnet*, 5(1), 1 – 8.

Kormann, R., and F. X. Meixner (2001), An analytical footprint model for non-neutral stratification, *Bound. Lay. Meteorol*, 99, 207 – 224.

Lee, T. W., J. Y. Lee, and Z. H. Wang (2012), Scaling of the urban heat island intensity using time-dependent energy balance, *Urban Clim.*, doi:10.1016/j.uclim.2012.10.005.

Loridan, T. and C. S. B. Grimmond (2012), Characterization of energy flux partitioning in urban environments: links with surface seasonal properties, *J. Appl. Meteorol. Climatol.*, 50, 185 – 202.

Massman, W. J. (2001), Reply to comment by Rannik on: "A simple method for estimating frequency response corrections for eddy covariance systems", *Agricultural and Forest Meteorology*, 107, 247 – 251.

Oke T. R. (2006) Initial guidance to obtain representative meteorological observations at urban sites. IOM Report No. 81. WMO/TD-No.1250.

Pierini, N.A., Vivoni, E.R., Robles-Morua, A., Scott, R.L., and Nearing, M.A. (2014), Using observations and a distributed hydrologic model to explore runoff threshold processes linked with mesquite encroachment in the Sonoran Desert. *Water Resour. Res*., 50(10): 8191–8215.

Schmid, H. P. (1994), Source areas for scalars and scalar fluxes, *Bound. Layer Meteorol.*, 54, 249 – 276.

Schmid, H. P. (1997), Experimental design for flux measurements: matching scales of observations and fluxes, *Agr. For. Meteorol.*, 87, 179 – 200.

Schmid, H. P. (2002), Footprint modeling for vegetation atmosphere exchange studies: a review and perspective, *Agr. For. Meteorol.*, 113, 159 – 183.

Van de Boer, A., A. F. Moene, D. Schuttemeyer, and A. Graf (2013), Sensitivity and uncertainty of analytical footprint models according to a combined natural tracer and ensemble approach, *Agr. For. Meteorol.*, *169*, 1 – 11.

Webb, E. K., G. I. Pearman, and R. Leuning (1980), Correction of flux measurements for density effects due to heat and water vapor transfer, *Quarterly J. Royal Meteorol. Soc.*, 106, 85 – 106.

Wilczak, J. M., S. P. Oncley, and S. A. Stage (2001), Sonic anemometer tilt correction algorithms, *Bound. Layer Meteorol.*, 99, 127 – 150.

Wilson, K., Goldstein, A., Falge, E., Aubinet, M., Baldocchi, D., Berbigier, P., Bernhofer, C., Ceulemans, R., Dolman, H., Field, C., Grelle, A., Ibrom, A., Law, B.E., Kowalski, A., Meyers, T., Moncrieff, J., Monson, R., Oechel, W., Tenhunen, J., Valentini, R., Verma, S., 2002. Energy balance closure at FLUXNET sites, *Agr. For. Meteorol.*, 113, 223-243.

Figure Captions

Figure 1. Three study site locations including (a) palo verde eddy covariance tower (PV-ECT) at ASU Tempe campus in a (b) xeric landscape consisting of palo verde trees with gravel surface that is drip irrigated, (c) parking lot eddy covariance tower (PL-ECT) at ASU Tempe campus on a (d) gravel area within the paved parking lot, near a high traffic intersection, and (e) turf grass eddy covariance tower (TG-ECT) near residential housing at ASU Polytechnic campus in Mesa, AZ in a (f) mesic landscape consisting of regularly irrigated turf grass. The 0.30 m aerial photographs in (b) are from USGS high resolution orthoimagery.

Figure 2. (a) Orthoimage centered at PV-ECT, with (b) the flux footprint of the ECT, representing 50% and 80% source area with (c) land cover classification consisting of: trees, grass, undeveloped – open land (gravel or bare soil), pavement, and buildings and concrete.

Figure 3. (a) Orthoimage centered at PL-ECT, with (b) the flux footprint of the ECT, representing 50% and 80% source area with (c) land cover classification consisting of: trees, grass, undeveloped – open land (gravel or bare soil), pavement, and buildings and concrete.

Figure 4. (a) Orthoimage centered at TG-ECT, with (b) the flux footprint of the ECT, representing 50% source area with (c) land cover classification consisting of: trees, grass, undeveloped – open land (gravel or bare soil), pavement, buildings and concrete, and residential buildings.

Figure 5. Meteorological variables measured at PV-ECT, including (a) air temperature at three different heights (low, medium, and high) and surface temperature, (b) incoming solar radiation (Is) and net radiation (Rn), (c) sensible (H), latent (LE) and ground (G) heat flux and (d)

volumetric soil moisture at 5 cm and 50 cm depths. Rainfall is plotted as the total accumulation [mm] per 30 minute time period.

Figure 6. Meteorological variables measured at PL-ECT, including (a) air temperature at three different heights (low, medium, and high) and surface temperature, (b) incoming solar radiation (Is) and net radiation (Rn), and (c) sensible (H) and latent (LE) heat flux. Rainfall is plotted as the total accumulation [mm] per 30 minute time period.

Figure 7. Meteorological variables measured at TG-ECT, including (a) air temperature at three different heights (low, medium, and high) and surface temperature, (b) incoming solar radiation (Is) and net radiation (Rn), (c) sensible (H), latent (LE) and ground (G) heat flux and (d) volumetric soil moisture at 5 cm, 15 cm and 50 cm depths.. Rainfall is plotted as the total accumulation [mm] per 30 minute time period.

Figure 8. Average diurnal cycle for energy balance fluxes [net radiation (Rn), sensible heat flux (H), latent heat flux (LE), and ground heat flux (G)] computed at 30 minute time steps over each ECT deployment duration at (a) PV-ECT (b) PL-ECT and (c) TG-ECT. Average rainfall is plotted and computed as the average rainfall amount for each 30 minute period during a day.

Figure 9. Sensible and latent heat ratios to net radiation minus ground heat radiation, (H/(Rn-G) and LE/(Rn-G), respectively), computed as an average daily value for (a) PV-ECT (b) PL-ECT and (c) TG-ECT.

Figure 10. Daily averaged carbon dioxide flux values at (a) PV-ECT (b) PL-ECT and (c) TG-ECT.

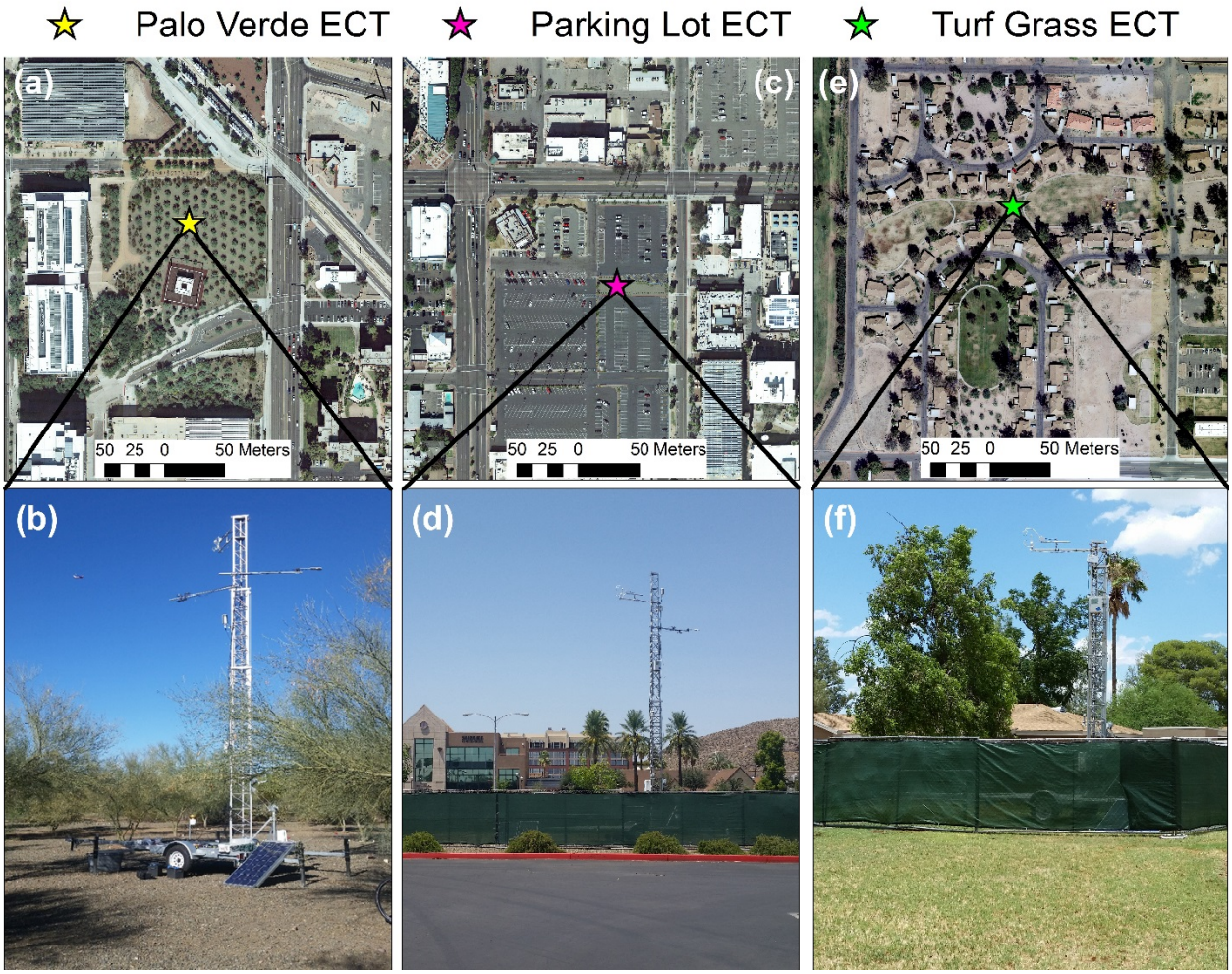
Palo Verde ECT
Parking Lot ECT
Turf Grass ECT
(a)
(b)
(c)
(d)
(e)
(f)
N
50 25 0 50 Meters
50 25 0 50 Meters
50 25 0 50 Meters

Figure 1

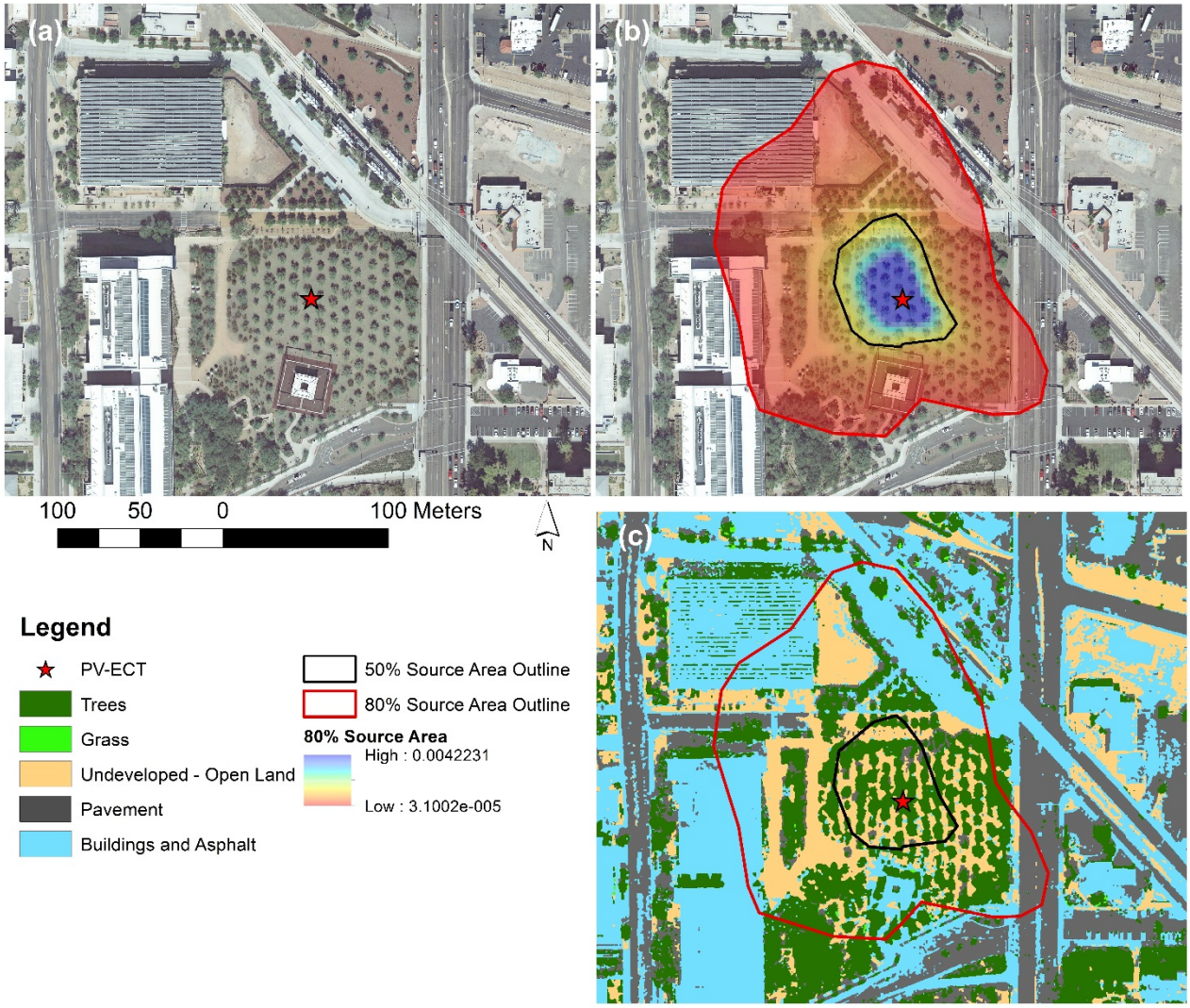
(a)
(b)
(c)
100 50 0 100 Meters
N
Legend
PV-ECT
Trees
Grass
Undeveloped - Open Land
Pavement
Buildings and Asphalt
50% Source Area Outline
80% Source Area Outline
80% Source Area
High : 0.0042231
Low : 3.1002e-005

Figure 2

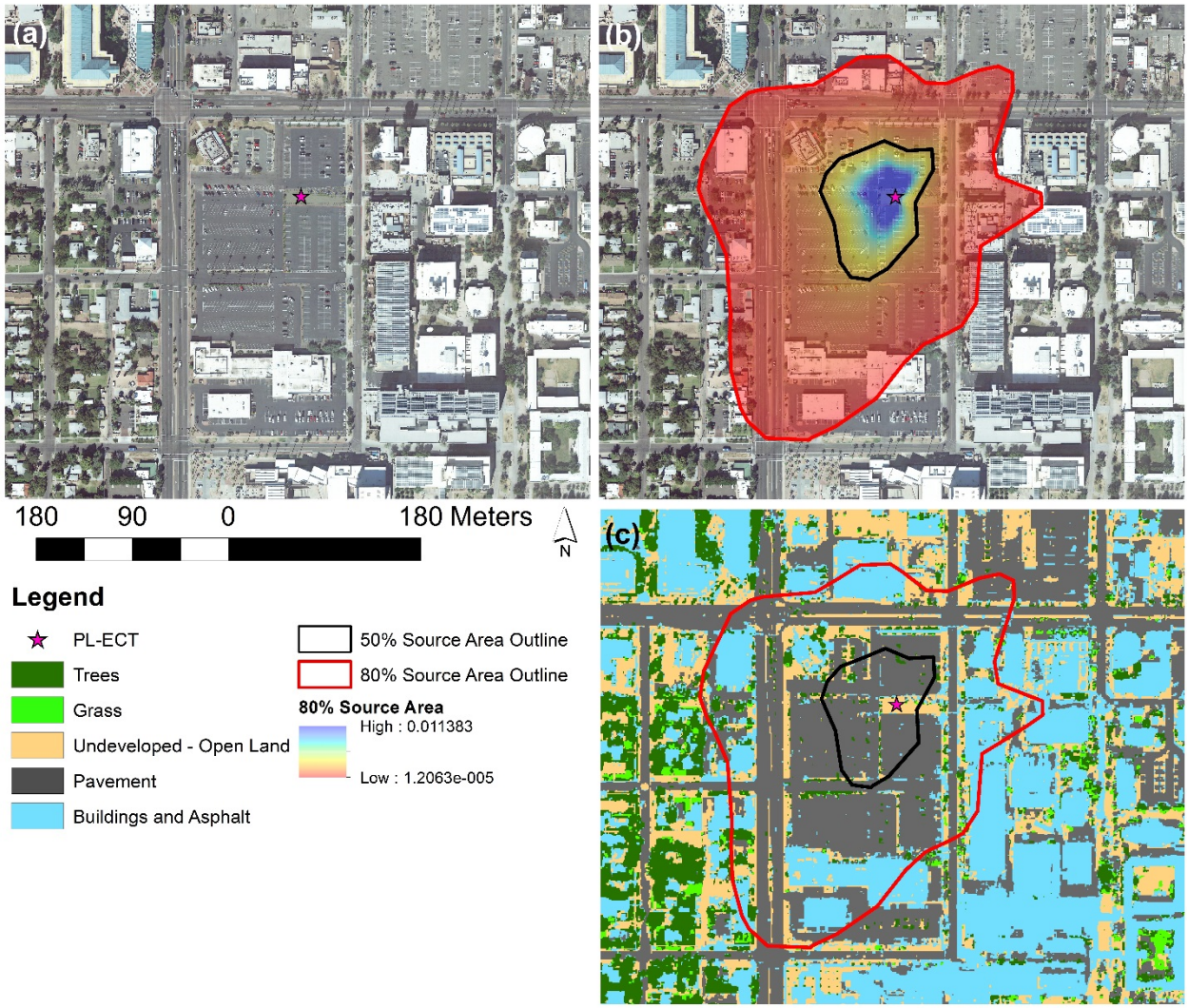
(a)
(b)
(c)
180 90 0 180 Meters
N
Legend
PL-ECT
Trees
Grass
Undeveloped - Open Land
Pavement
Buildings and Asphalt
50% Source Area Outline
80% Source Area Outline
80% Source Area
High : 0.011383
Low : 1.2063e-005

Figure 3

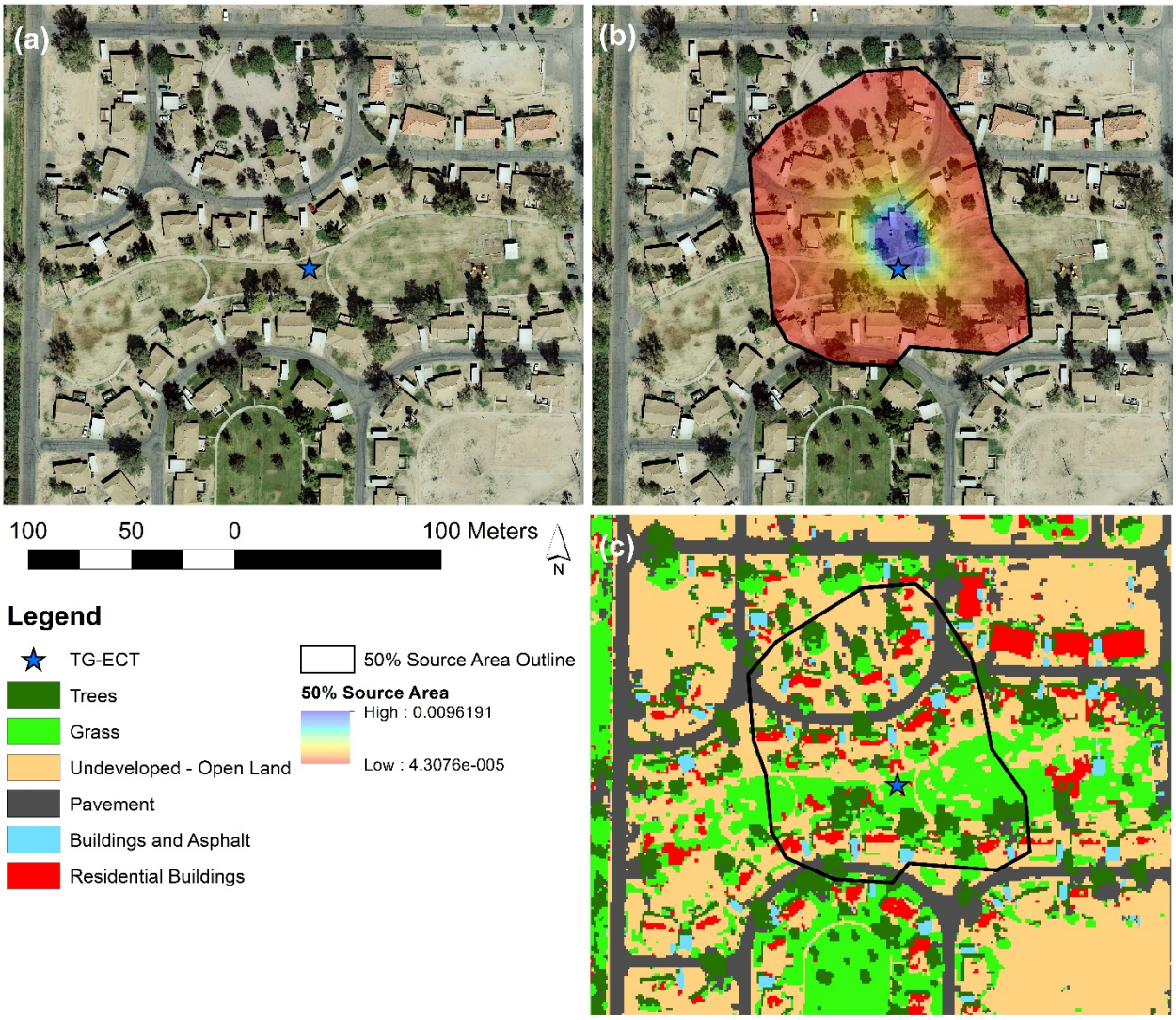
(a)
(b)
(c)
100 50 0 100 Meters
N
Legend
TG-ECT
Trees
Grass
Undeveloped - Open Land
Pavement
Buildings and Asphalt
Residential Buildings
50% Source Area Outline
50% Source Area
High : 0.0096191
Low : 4.3076e-005

Figure 4

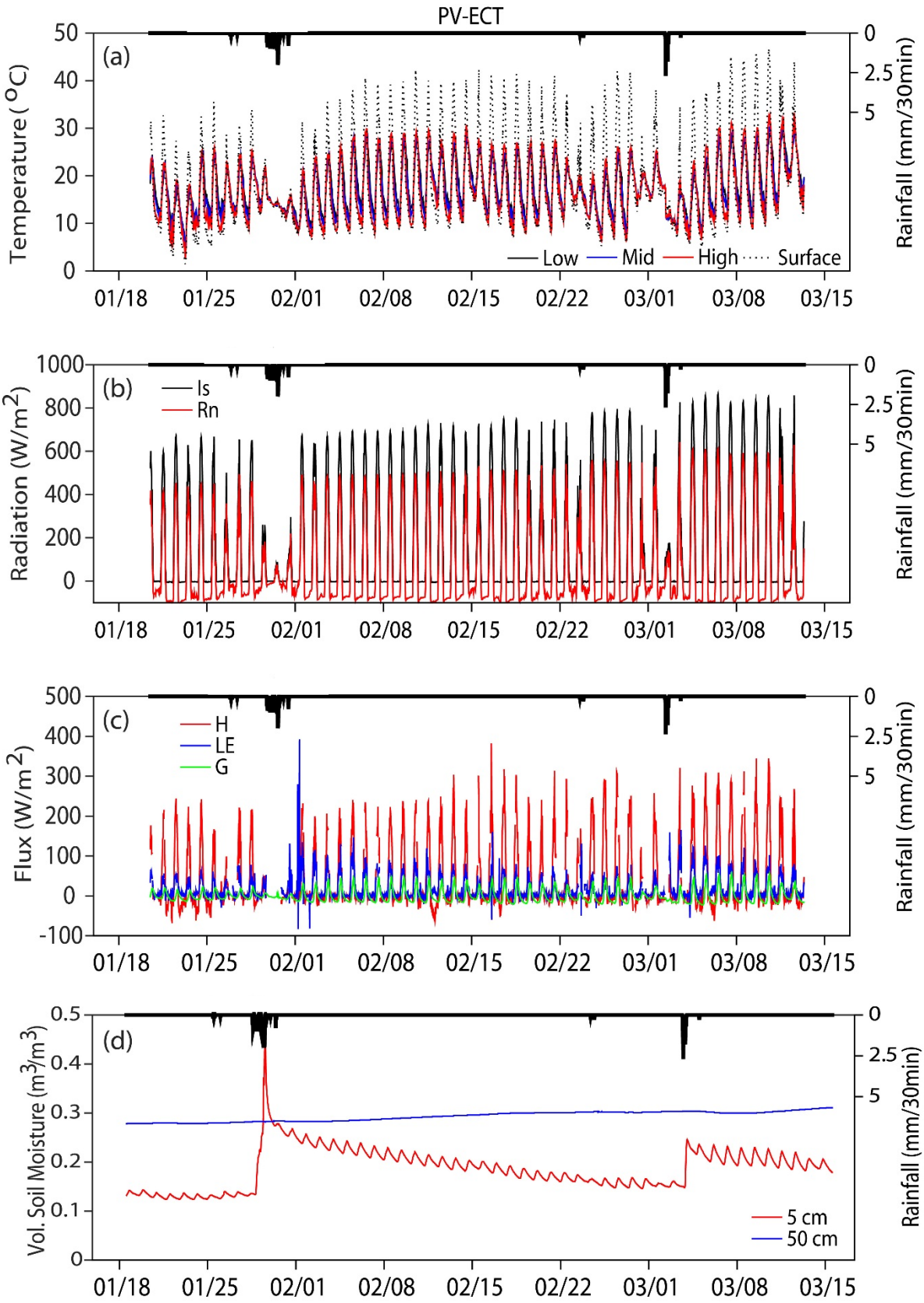
PV-ECT
(a)
Temperature (°C)
Rainfall (mm/30min)
Low
Mid
High
Surface
(b)
Radiation (W/m2)
Is
Rn
(c)
Flux (W/m 2)
H
LE
G
(d)
Vol. Soil Moisture (m3/m3)
5 cm
50 cm
01/18
01/25
02/01
02/08
02/15
02/22
03/01
03/08
03/15

Figure 5

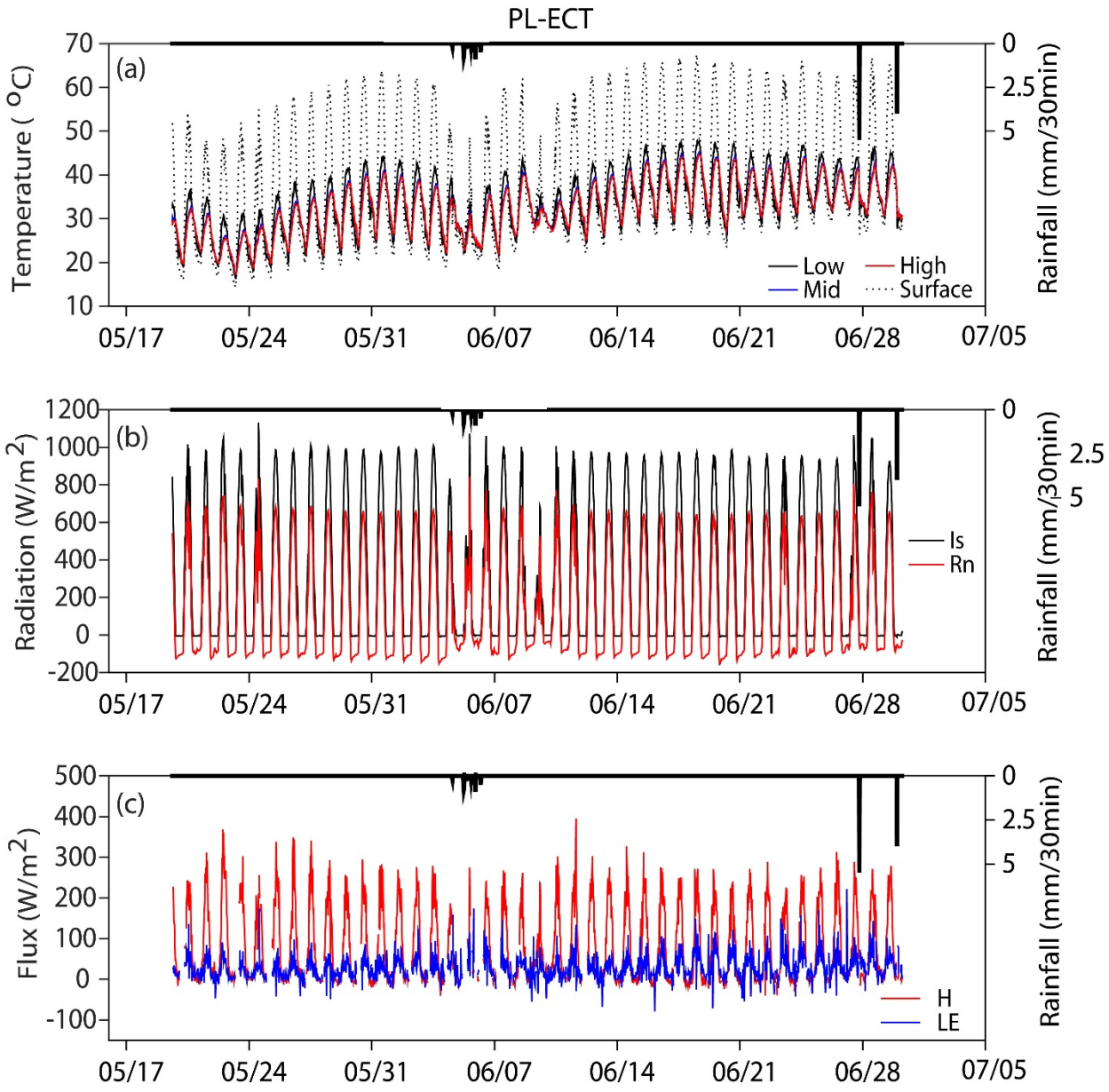
PL-ECT
(a)
Temperature (°C)
Rainfall (mm/30min)
Low
High
Mid
Surface
(b)
Radiation (W/m2)
Is
Rn
(c)
Flux (W/m2)
H
LE
05/17
05/24
05/31
06/07
06/14
06/21
06/28
07/05

Figure 6

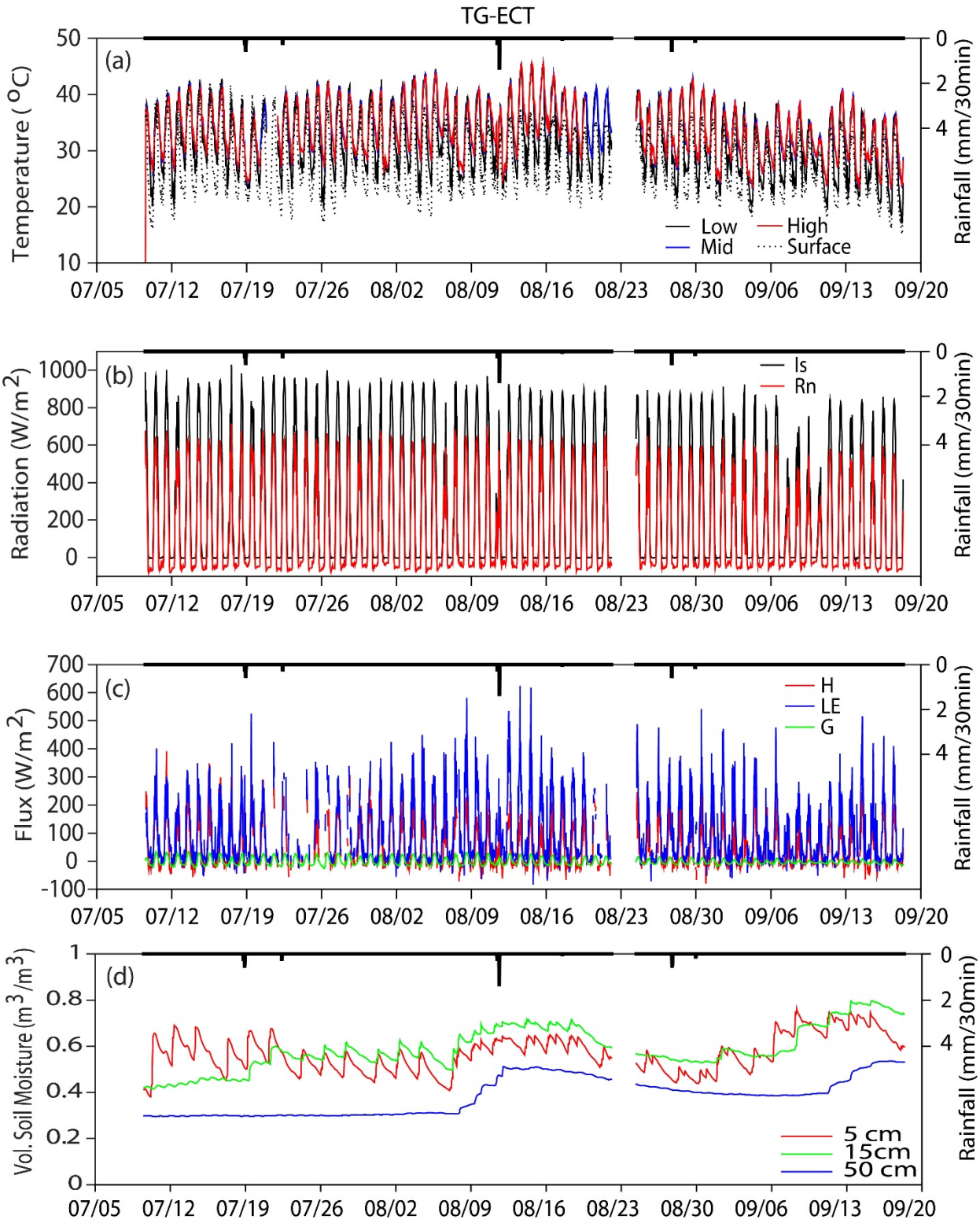
TG-ECT
(a)
Temperature (°C)
Rainfall (mm/30min)
Low
High
Mid
Surface
(b)
Radiation (W/m 2)
Is
Rn
(c)
Flux (W/m 2)
H
LE
G
(d)
Vol. Soil Moisture (m 3/m 3)
5 cm
15cm
50 cm
07/05
07/12
07/19
07/26
08/02
08/09
08/16
08/23
08/30
09/06
09/13
09/20

Figure 7

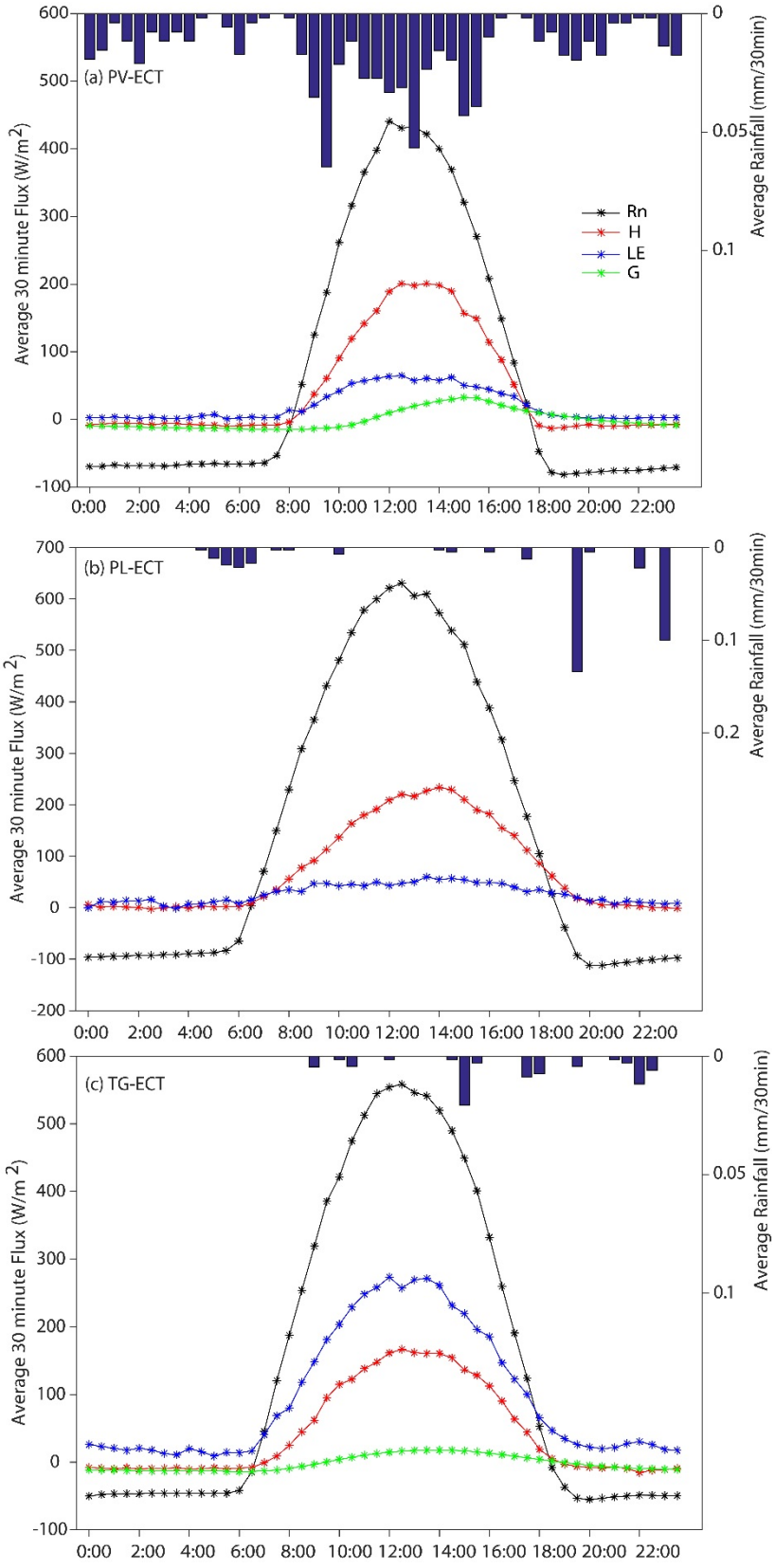
(a) PV-ECT
Rn
H
LE
G
Average 30 minute Flux (W/m 2)
Average Rainfall (mm/30min)
(b) PL-ECT
Average 30 minute Flux (W/m 2)
Average Rainfall (mm/30min)
(c) TG-ECT
Average 30 minute Flux (W/m 2)
Average Rainfall (mm/30min)
0:00 2:00 4:00 6:00 8:00 10:00 12:00 14:00 16:00 18:00 20:00 22:00

Figure 8

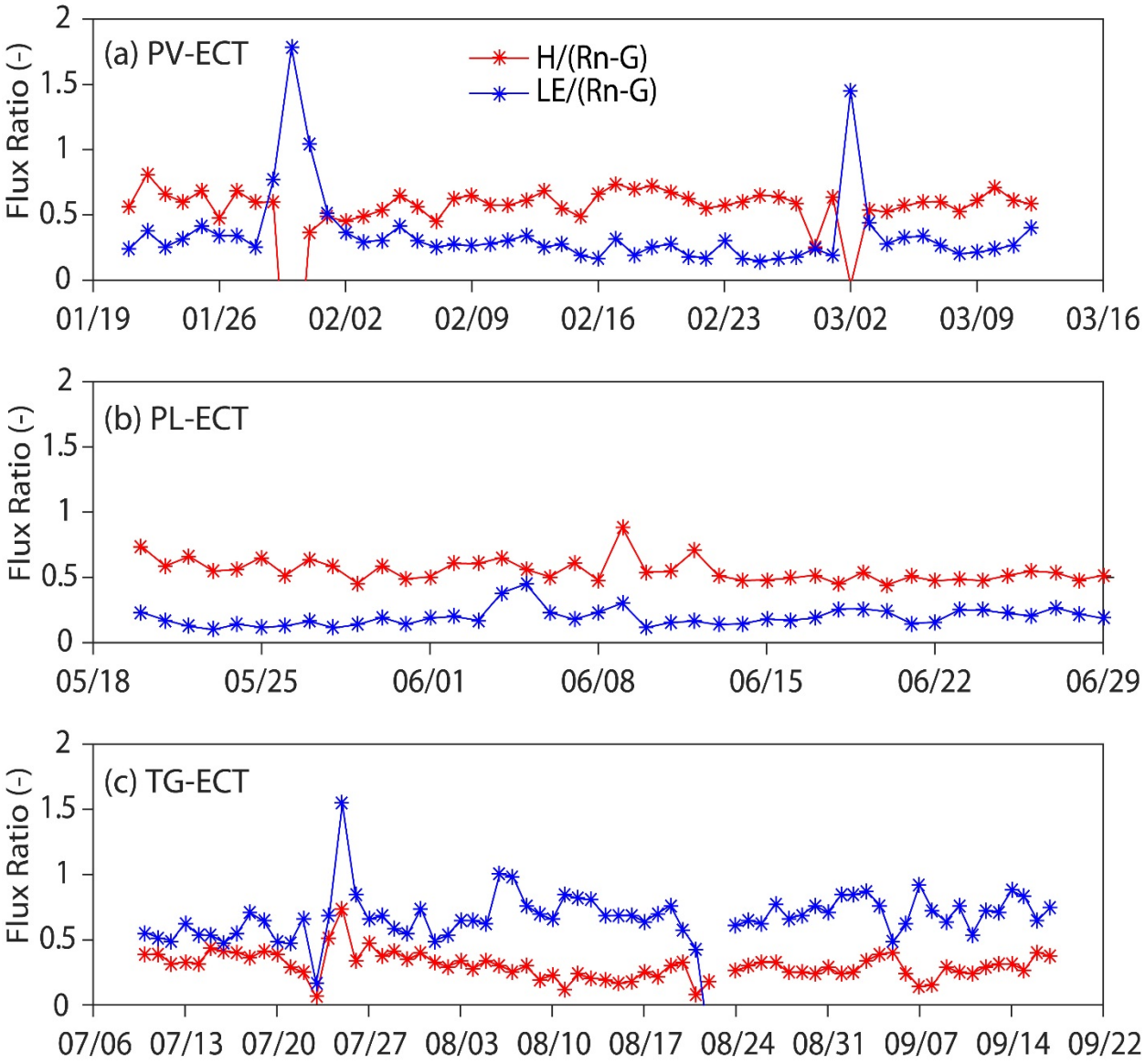
(a) PV-ECT
H/(Rn-G)
LE/(Rn-G)
Flux Ratio (-)
2
1.5
1
0.5
0
01/19
01/26
02/02
02/09
02/16
02/23
03/02
03/09
03/16
(b) PL-ECT
Flux Ratio (-)
05/18
05/25
06/01
06/08
06/15
06/22
06/29
(c) TG-ECT
Flux Ratio (-)
07/06
07/13
07/20
07/27
08/03
08/10
08/17
08/24
08/31
09/07
09/14
09/22

Figure 9

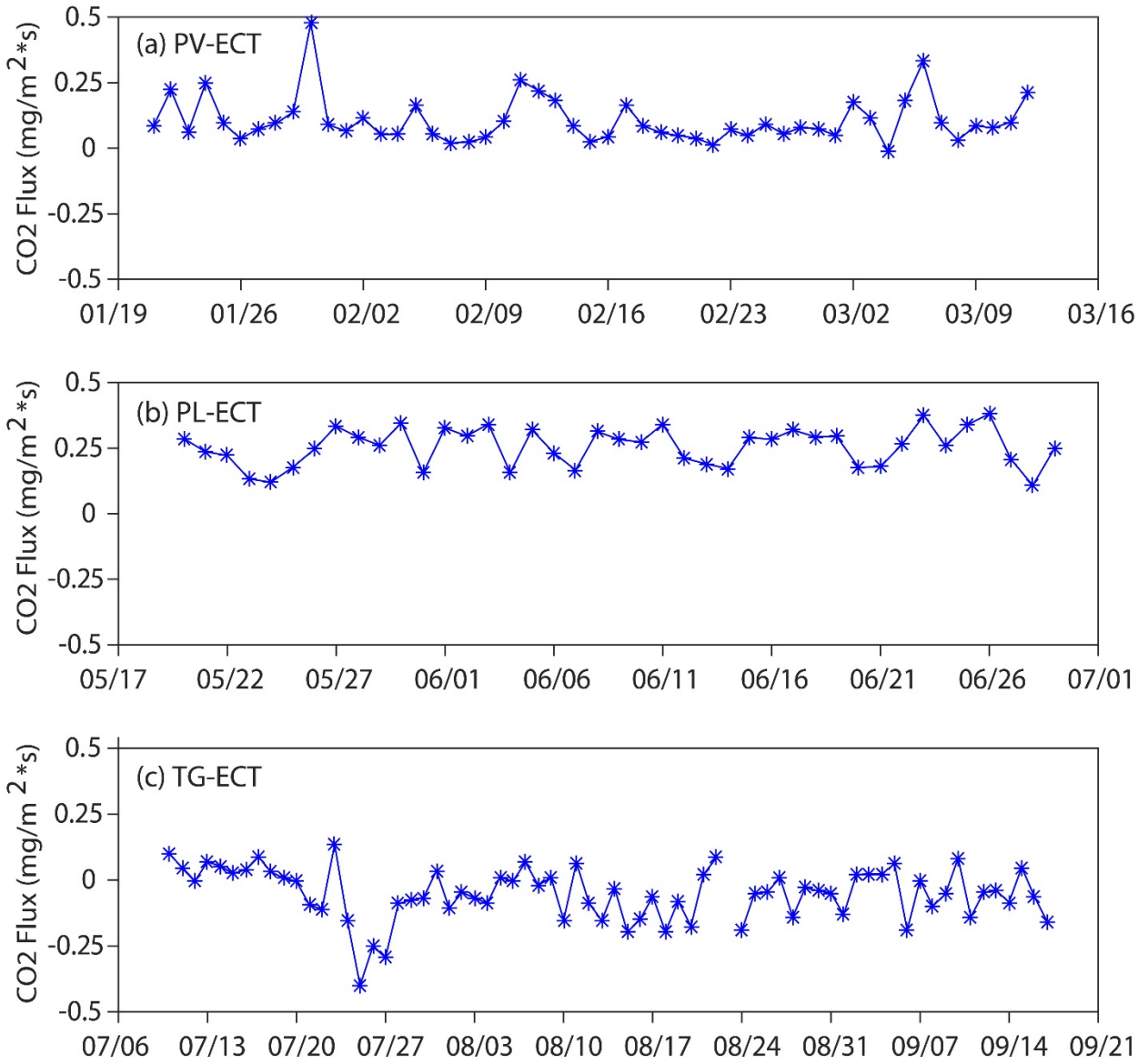
(a) PV-ECT
(b) PL-ECT
(c) TG-ECT
CO2 Flux (mg/m 2 *s)
0.5
0.25
0
-0.25
-0.5
01/19
01/26
02/02
02/09
02/16
02/23
03/02
03/09
03/16
05/17
05/22
05/27
06/01
06/06
06/11
06/16
06/21
06/26
07/01
07/06
07/13
07/20
07/27
08/03
08/10
08/17
08/24
08/31
09/07
09/14
09/21

Figure 10

Table Captions

Table 1. General characteristics for the three study sites, including land cover description, location, and elevation.

Table 2. Eddy covariance deployment specifications for the three study sites, including angle and height the high frequency sensors were mounted at, speed at which EC measurements were being taken, and each deployment duration.

Table 3. Land cover percentages determined within 50% and 80% source areas for each site. Area values in square meters for 50% and 80% source area at each site and the percent of the flux that falls within the specified 300 m fetch.

Table 4. Dates of rainfall events that occurred during the deployment period at each tower, with approximate start and ending times and total accumulation.

Table 5. Average evaporative fraction, Bowen ratio, sensible heat flux fraction of net radiation minus ground heat flux, and latent heat flux fraction of net radiation minus ground heat flux for the three sites. Evaporative fraction and Bowen ratio were calculated at noon each day, while the daily average flux values were used to find the fraction values. Averages were then computed over each ECT deployment period.

[a]PL-ECT had no G measurement, therefore G was assumed to equal zero.

Table 6. Evaporative fraction, Bowen ratio, sensible heat flux fraction of net radiation minus ground heat flux, and latent heat flux fraction of net radiation minus ground heat flux for the three sites. Evaporative fraction and Bowen ratio were calculated at noon each day, while the daily average flux values were used to find the fraction values. Averages were then computed

over wet days, defined as a day where rainfall occurred plus three days after, and dry days, defined as all days that are not classified as wet. Averages were also computed for rainfall events that occurred during the day time (Wet-Day) including three days after, where Dry-Day is all other days that were not classified as Wet-Day.

[a]PL-ECT had no G measurement, therefore G was assumed to equal zero.

Table 1. General characteristics for the three study sites, including land cover description, location, and elevation.

Site	Land Cover	UTM Easting (m)	UTM Northing (m)	Latitude	Longitude	Elevation (m)
PV-ECT	Palo Verde	413797	3698213	33.4198	-111.9272	354
PL-ECT	Pavement	412725	3698373	33.4212	-111.9387	356
TG-ECT	Turf Grass	436646	3686041	33.3116	-111.6806	411

Table 1

Table 2. Eddy covariance deployment specifications for the three study sites, including angle and height the high frequency sensors were mounted at, speed at which EC measurements were being taken, and each deployment duration.

Site	Angle (deg)	Measurement Height (m)	Speed	Start Time	End Time	Days
PV-ECT	21	7	20 Hz	1/20/2015 12:00	3/13/2015 8:30	53
PL-ECT	227	9	10 Hz	5/19/2015 15:00	6/30/2015 6:00	43
TG-ECT	230	8	10 Hz	7/9/2015 13:00	9/18/2015 8:30	74

Table 2

Table 3. Land cover percentages determined within 50% and 80% source areas for each site. Area values in square meters for 50% and 80% source area at each site and the percent of the flux that falls within the specified 300 m fetch.

	PV-ECT		PL-ECT		TG-ECT
	50% Source Area	**80% Source Area**	**50% Source Area**	**80% Source Area**	**50% Source Area**
Trees	55.6%	37.0%	4.3%	5.5%	17.9%
Grass	0.0%	0.2%	0.2%	0.7%	23.6%
Undeveloped	36.6%	27.9%	10.0%	14.8%	36.5%
Pavement	5.6%	26.5%	82.9%	56.0%	11.5%
Buildings/Concrete	2.2%	26.5%	2.5%	23.0%	2.6%
Residential	0.0%	0.0%	0.0%	0.0%	7.9%
Area [m^2]	1,917	15,066	9,243	76,158	14,346
% in 300 m fetch	96.2%		90.1%		61.1%

Table 3

Table 4. Dates of rainfall events that occurred during the deployment period at each tower, with approximate start and ending times and total accumulation.

PV-ECT			PL-ECT			TG-ECT		
Date	**Time**	**P [mm]**	**Date**	**Time**	**P [mm]**	**Date**	**Time**	**P [mm]**
1/26/2015	20:30-23:30	0.6	6/4/2015	14:00-14:30	0.3	7/18/2015	19:30-22:30	1.5
1/27/2015	9:30	0.1	6/5/2015	5:30-10:00	2.5	7/22/2015	9:00	0.3
1/29/2015	18:00-23:30	5.3	6/5/2015	16:00-17:30	0.7	8/11/2015	10:00-10:30	0.4
1/30/2015	0:00-20:00	18.5	6/5/2015	22:00-23:00	1	8/11/2015	14:30	0.1
1/31/2015	11:00-12:00	1.2	6/6/2015	4:30-6:00	1	8/11/2015	22:00-22:30	1.6
2/23/2015	19:30-21:00	0.7	6/27/2015	19:30-20:00	5.7	8/27/2015	17:30-18:00	1.1
3/2/2015	8:30-16:00	11.9	6/29/2015	23:00	4	8/29/2015	22:00-22:30	0.3
3/3/2015	14:00	0.3						

Table 4

Table 5. Average evaporative fraction, Bowen ratio, sensible heat flux fraction of net radiation minus ground heat flux, and latent heat flux fraction of net radiation minus ground heat flux for the three sites. Evaporative fraction and Bowen ratio were calculated at noon each day, while the daily average flux values were used to find the fraction values. Averages were then computed over each ECT deployment period.
[a]PL-ECT had no G measurement, therefore G was assumed to equal zero.

Site	Evaporative Fraction [-]	Bowen Ratio [-]	H/(Rn-G) [-]	LE/(Rn-G) [-]
PV-ECT	0.27	3.05	0.54	0.36
PL-ECT[a]	0.16	8.01	0.55	0.20
TG-ECT	0.61	0.53	0.30	0.67

Table 5

Table 6. Evaporative fraction, Bowen ratio, sensible heat flux fraction of net radiation minus ground heat flux, and latent heat flux fraction of net radiation minus ground heat flux for the three sites. Evaporative fraction and Bowen ratio were calculated at noon each day, while the daily average flux values were used to find the fraction values. Averages were then computed over wet days, defined as a day where rainfall occurred plus three days after, and dry days, defined as all days that are not classified as wet. Averages were also computed for rainfall events that occurred during the day time (Wet-Day) including three days after, where Dry-Day is all other days that were not classified as Wet-Day.
[a]PL-ECT had no G measurement, therefore G was assumed to equal zero.

	Evaporative Fraction [-]				**Bowen Ratio [-]**			
Condition	**Wet**	**Dry**	**Wet-Day**	**Dry-Day**	**Wet**	**Dry**	**Wet-Day**	**Dry-Day**
PV-ECT	0.29	0.26	0.32	0.25	3.0	3.1	2.0	3.3
PL-ECT	0.21	0.15	0.22	0.15	4.1	9.1	3.6	8.8
TG-ECT	0.62	0.61	0.69	0.61	0.65	0.49	0.47	0.53
	H/(Rn-G) [-]				**LE/(Rn-G) [-]**			
Condition	**Wet**	**Dry**	**Wet-Day**	**Dry-Day**	**Wet**	**Dry**	**Wet-Day**	**Dry-Day**
PV-ECT	0.45	0.59	0.33	0.59	0.44	0.31	0.52	0.29
PL-ECT[a]	0.58	0.54	0.61	0.54	0.27	0.17	0.30	0.18
TG-ECT	0.27	0.31	0.23	0.31	0.67	0.67	0.67	0.67

Table 6